A Study on the Shunt Effect in Resistance Spot Welding

The proposed model can be used to compensate for shunt effect by adjusting weld current

BY H. S. CHANG AND H. S. CHO

ABSTRACT. One of the important factors affecting the weld quality of practical resistance spot welding is the shunt effect, which deteriorates weld quality due to the shunt current that flows through neighboring welds. Although some experimental studies for compensation of its effect have been presented, no effort has been made to establish an analytical model that can predict the effect of shunt mechanism on the weld quality. This paper presents an analytical model by which the shunt effect upon the nugget growing behavior can be analyzed. The voltage field and temperature distribution in the weldment are computed by the proposed three-dimensional finite difference numerical model. Experimental verification of the calculated results was also performed and discussed in detail. The comparison of both results shows that the proposed thermal-electric model can predict the shunt effect fairly well.

Introduction

In the resistance spot welding (RSW) process, resistance heating occurs at the interface due to the passage of a high current through the electrodes and the workpieces. In normal practice, to obtain a desired heating condition, the welding current, pressure applied to the workpiece and weld time are preset for a particular application, depending upon the material properties of the workpiece to be welded and the electrode tip geometry. However, even when the machine variables are held at the desired condition, there is often considerable variation in weld quality from part to part. This is due to variations in welding current caused by changes in the surface condition of the workpieces, changes in the electrode tip diameter fitup and changes in the impedance of the welding circuit.

In practical welding situations, welding is done one after another, and thus the adjacent weld affects the quality of the subsequent weld due to a shunt current that flows through the existing spot welds. This effect is called shunt effect and is known to be a major source of quality variation. Among many experimental studies on the shunt effect, Hard (Ref. 3) has reported that tests of welds made at various shunt spacings in a single row of spot welded joints characteristically show a decline in the tension-shear strength per weld at the closer spacings. He has proposed a method of measuring shunt path resistance, but no direct correlation of shunt path resistance and weld current level necessary to compensate for shunt effect was available in his study. According to the study by Blair (Ref. 4), the shunt effect is found to be affected by such factors as welding machine impedance, spot spacing, sheet width, location of shunt path and sheet temperature. Nippes, *et al.* (Ref. 5), investigated the measurement of the shunt current and the effect of spot spacing, electrode and backing bar geometries, weld material preparation and electrode force on the shunt current in the series spot welding. Johnson (Ref. 6) proposed that the necessary minimum spacing between adjacent spot welds be enough to prevent shunting or to limit it to an acceptable amount.

KEY WORDS

Resistance Spot Welding
Shunt Effect/Spacing
Analytical Model
Nugget Growth/Size
RWMA Cl II Electrode
Voltage Variations
Current Variations
Resistance Variation
Temperature Distribution
Thermoelectrical model

The many problems associated with the shunt effect necessitate a comprehensive analytical investigation of it, since no analytical effort has been made due to the highly complicated phenomena in the thermal and electrical behavior of the RSW process. In the case of welding a single spot, several authors have attempted to successfully present a numerical model that can predict the thermomechanical behavior in the weldment during RSW. Recently, Nied (Ref. 7) developed an extensive model that includes the thermomechanical coupling aspects in the RSW process. Despite his insufficient analysis of the various contact resistances in the weldment, his model was applied toward a general understanding of the the RSW process, especially the prediction of the mechanical deformation. A one-dimensional model that includes the contact resistances and the effective heat transfer in the molten pool was developed by Gould (Ref. 8). In his model, due to limitation of one-dimensional analysis and lack of sufficient data concerning the interface resistance between two weldments, the relation between the welding variables and the nugget geometry could not be explained in detail. A more realistic study by Cho (Ref. 9) developed an analytical model to predict the thermal behavior in the weldment with weld time, taking into account the complicated thermal-electric interaction at the interface as well as the temperature and the voltage distribution in the weldment.

In this study, a comprehensive investigation of the spot welding process with the shunt effect is made in order to provide an analytical model that can theoretically predict the effect of the shunting phenomenon on the growth of the nugget. In this model, the shunt effect is taken into account by introducing the shunt circuit made by an adjacent nugget when welding is done one after another. A series of simulations was performed to predict the time behavior of the voltage fields

H. S. CHANG is Associate Professor, Department of Mechanical Engineering, Myong Ji University, Yong-In, Kyung-Gi, Korea. H. S. CHO is Professor, Department of Production Engineering, Korea Advanced Institute of Science and Technology, Chongryangri, Seoul, Korea.

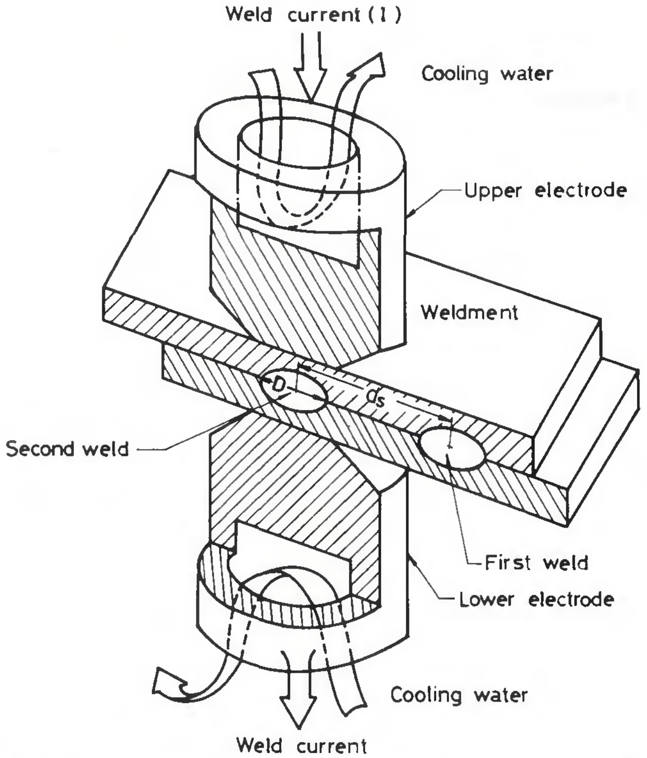

Fig. 1 — Schematic diagram of spot welding process in the presence of shunt effect (shunt spacing = d_s).

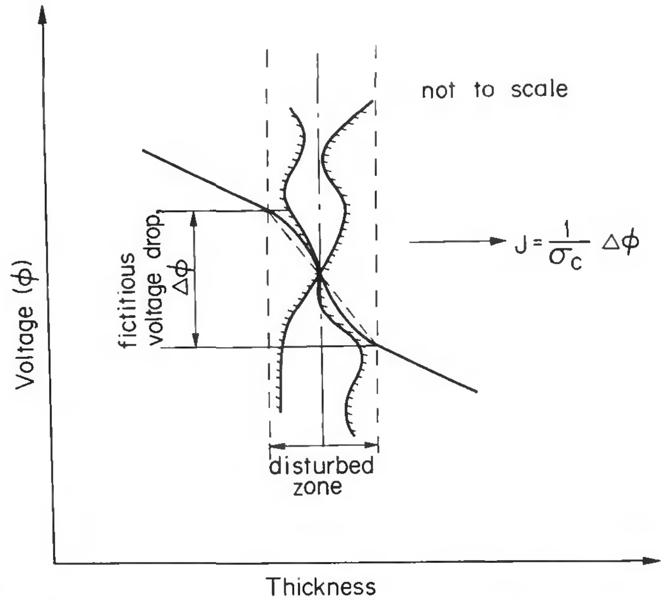

Fig. 2 — Model of contact surface in resistance spot welding (not to scale).

and the temperature distribution across the weldment for various shunt spacings. To obtain the temperature and the voltage potential field in the weldment, the alternating direction implicit (ADI) method was used as a numerical scheme. The numerically obtained results include the nugget growth behavior with the shunt spacing, amount of welding current shunted through an adjacent weld, and the resulting voltage and temperature distributions. A series of experiments was also performed to verify the results predicted by the model. The comparisons of the experimental and numerical results are discussed in detail.

Formulation of the Numerical Model

The resistance spot welding mechanism in the presence of the shunt effect is illustrated schematically in Fig. 1. In resistance spot welding, required heat is generated by passage of a high current pulse across the weldment interface and base metal. When the weldment is connected to the two electrodes and the electric loading is applied, the voltage potential field is established within it and along the interface dependent upon the voltage drop between the electrode and the welding interface. Then, this voltage distribution causes a current flow, and the corresponding current density is given by

$$J = \frac{1}{\sigma(T)} \nabla \phi \qquad (1)$$

where J is the current density vector, $\sigma(T)$ is the resistivity of the base metal dependent on the temperature T, and ϕ is the voltage across the electrodes.

The Behavior of the Interface in Weldment

The interface in the weldment represents a microcontact between elements, with its contacting surfaces characterized by roughness and waviness. The convergence of the electric current flow lines toward these microcontact points (asperities) results in an electric constriction resistance. The constriction resistance at the interface causes a voltage drop across it and generates heat to fuse the workpieces. The electrical resistance at the interface changes greatly during the welding process, depending on the metallurgical and mechanical properties of the material adjacent to the interface, and the pressure and the temperature distributions that strongly affect these properties (Refs. 10, 11). With the complicated thermo-electric behavior of the contact taken into consideration, and the thermal and electric boundary conditions imposed on the problem, a suitable idealization for the characteristics of the interface is necessary to deal with the problem.

As current flows across the interface, the voltage distribution in a plane normal to the interface seems to be discontinuous. Actually, this is not true and the sharp voltage drop between extrapolated voltage values on either side of the interface is a fictitious interface voltage drop (Ref. 9) as shown in Fig. 2. Hence, it is reasonable to assume a linear voltage profile within the disturbed zone, thus maintaining a continuity in the voltage potential field. Then, idealization of the interface of electric current flow can be done by assigning an averaged contact resistivity, from the microscopic point of view. The current density across the interface of unit area, J, is given by

$$J = \frac{1}{\sigma} \frac{\partial \phi}{\partial n} = \frac{1}{\sigma_c} \Delta\phi \qquad (2)$$

where σ_c is the interfacial resistivity, n is the normal vector-to-interface plane and $\Delta\phi$ is the voltage drop at the interface. In the above, the averaged contact resistance assigned between the base metal and normal plane is selected in such a way that current flow through the boundary between the disturbed zone and base metal maintains an equilibrium state.

According to the work by Tslaf (Ref. 11), variation of the contact resistance is in direct proportion to the square root of the corresponding hardness value as follows:

$$\sigma_c = \sigma_c(T_o, P) \sqrt{\frac{H(T)}{H(T_o)}} \qquad (3)$$

where H is the hardness, T is the temperature and $\sigma_c(T_o,P)$ is the interfacial resistivity at room temperature T_o under the pressure P by the electrode force. The hardness is a decreasing function of temperature, and the variation of hardness is illustrated in Ref. 12 for mild steel and copper. Then, the heat generation at the interface, q, becomes

$$q = \frac{1}{\sigma_c}(\Delta\phi)^2 \quad (4)$$

Voltage Potential Distribution

In this section, the voltage distribution in the weldment is examined, taking into account the adjacent weld (shunt circuit). The voltage distribution is not only used to calculate the heat generation in the weldment for the analysis of thermal behavior, but also to obtain the shunt current variation during welding. To obtain the voltage distribution the following assumptions are made:

1) Voltage drop in the electrode can be neglected compared with that in the weldment, since the electrical conductivity of the electrode is an order of magnitude higher than that of the weldment.

2) The magnetic stirring effect in the nugget (Ref. 13) is not considered.

3) At the beginning of welding, the initial contact area between the two weldments is the same as that of weldment/electrode contact. As heating progresses with the welding cycle, radial enlargement in the contact area is assumed to take place along the isothermal line of 723°C (1333°F) in the weldment/weldment interface, where the weldment material is collapsed due to softening with the increase in temperature.

4) The contact resistance is directly proportional to the square root of the hardness value as explained previously in Equation 3.

5) To avoid computational burdens, the cross-sectional area of the preweld nugget (the first nugget) is simplified as rectangular (solid line), although the area of the actual weld is circular (dotted line) as shown in Fig. 3.

Under these assumptions, the following quasi-Laplace equation governing the voltage potential, $\phi_{(x,y,z)}$, can be written in the rectangular coordinates as:

$$\frac{\partial}{\partial x}\left[\frac{1}{\sigma}\frac{\partial\phi}{\partial x}\right] + \frac{\partial}{\partial y}\left[\frac{1}{\sigma}\frac{\partial\phi}{\partial y}\right] + \frac{\partial}{\partial z}\left[\frac{1}{\sigma}\frac{\partial\phi}{\partial z}\right] = 0 \quad (5)$$

and referring to Fig. 3, the boundary conditions are given by:

1) At the interface between two weldments (z = 0),

$$\frac{1}{\sigma}\frac{\partial}{\partial z}\phi_{(x,y,0)} = \frac{1}{\sigma_w/2}\left[\phi_{(x,y,0)} - \phi_n\right] \quad (6a)^{(1)}$$

at $XE1 < x < XE2,\ 0 < y < YE(x)$

$$\phi_{(x,y,0)} = \phi_n \quad (6b)$$

at $XS1 < x < XS2,\ 0 < y < YS$

2) At the interface between the electrode and the weldment (z = L1),

$$\frac{1}{\sigma}\frac{\partial}{\partial z}\phi_{(x,y,L_1)} = \frac{1}{\sigma_e}\left[\phi_e - \phi_{(x,y,L_1)}\right] \quad (6c)$$

at $XE1 < x < XE2,\ 0 < y < YE(x)$

3) From the geometric symmetry,

$$\frac{1}{\sigma}\frac{\partial}{\partial y}\phi_{(x,0,z)} = 0 \quad (6d)$$

4) At the air-contact surface,

$$\frac{\partial\phi}{\partial n} = 0 \quad (6e)$$

where ϕ is the voltage potential of the weldment, ϕ_n is the voltage potential at the center of the interface between two weldments, ϕ_e is the voltage potential of the electrode, σ is the resistivity of the weldment, σ_w is the interfacial resistivity between two weldments, σ_e is the interfacial resistivity between the electrode and the weldment, and n is the vector normal to the interface.

Temperature Distribution in the Weldment

Numerical modeling of thermal behavior in the weldment and electrode needs the following assumptions:

1) The variation of thermal properties of the weldment due to the electrode squeeze force is neglected.

2) The heat generation in the electrode can be neglected since the voltage drop in electrode is negligibly small.

3) Free convection heat loss at the surface, except at the contact interface, is neglected, compared with the heat loss due to the cooling water.

4) Heat is conducted only in the Z-direction at the interface of electrode/weldment and weldment/weldment contact.

In the following equations ρ, c and k are density, specific heat and thermal conductivity, respectively, $\nabla\phi$ is the gradient of voltage potential, T_∞ is the cooling water temperature (15°C/59°F). The subscripts w and e denote the weldment and the electrode, respectively. The other geometric parameters such as L1, L2, XE1, XE2 and YE(x) are given in Fig. 3.

Then, the temperature distribution, T_w, in the weldment is described as an unsteady heat conduction problem with heat generation term as follows:

$$\rho_w c_w \frac{\partial T_w}{\partial t} = \frac{\partial}{\partial x}\left[k_w\frac{\partial T_w}{\partial x}\right] + \frac{\partial}{\partial y}\left[k_w\frac{\partial T_w}{\partial y}\right] + \frac{\partial}{\partial z}\left[k_w\frac{\partial T_w}{\partial z}\right] + \frac{1}{\sigma}\nabla\phi\cdot\nabla\phi \quad (7)$$

and the temperature distribution in the electrode, Te, is

$$\rho_e c_e \frac{\partial T_e}{\partial t} = \frac{\partial}{\partial x}\left[k_e\frac{\partial T_e}{\partial x}\right] + \frac{\partial}{\partial y}\left[k_e\frac{\partial T_e}{\partial y}\right] + \frac{\partial}{\partial z}\left[k_e\frac{\partial T_e}{\partial z}\right] \quad (8)$$

From the Equations 6a–e and the Assump-

(1) ***Factor of 2 in the Equation (6A): An Explanation***—*σ_w means the interfacial resistivity between two weldments (across two weldments). The voltage potential term, ϕ_n doesn't come from the interfacial resistance. It is an imaginary voltage potential at the center of the interface between two weldments introduced for the generality of this program, especially to assign specific voltage potential value to the previous spot weld (shunt circuit). In actual computation for this paper, ϕ_n was set equal to zero. Since the voltage potential is ϕ_n at the center of interface (z = 0), the voltage drop across the interface between two weldments is: $\phi(x,y,+0) - \phi(x,y,-0) = 2(\phi(x,y,+0) - \phi_n)$. Hence, the factor of 2 is necessary in the Equation 6a.*

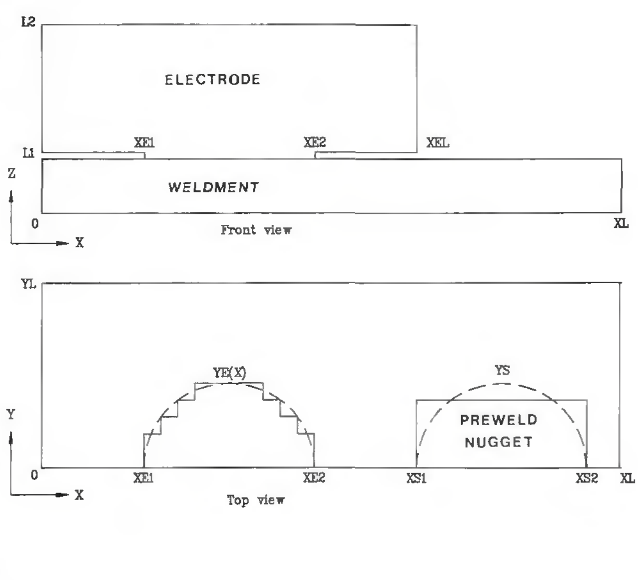

Fig. 3 — Projective views of electrode and weldment for FDM modeling.

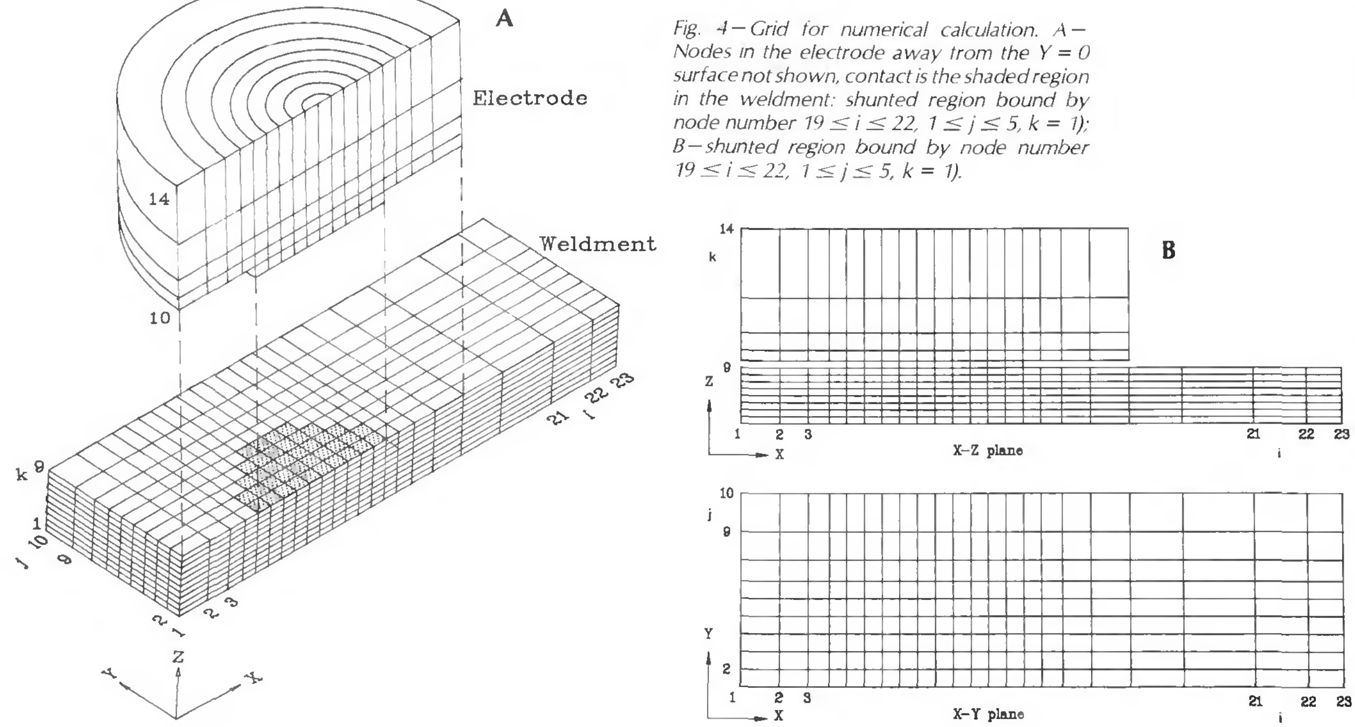

Fig. 4 — Grid for numerical calculation. A — Nodes in the electrode away from the Y = 0 surface not shown, contact is the shaded region in the weldment: shunted region bound by node number $19 \leq i \leq 22$, $1 \leq j \leq 5$, $k = 1$); B — shunted region bound by node number $19 \leq i \leq 22$, $1 \leq j \leq 5$, $k = 1$).

tion 4, the boundary conditions are as follows (Fig. 3):

1) At the interface between two weldments (z = 0),

$$-k_w \frac{\partial}{\partial z} T_{w(x,y,0)} = \frac{1}{\sigma_w/2} (\phi_{(x,y,0)} - \phi_n)^2 \quad (9a)$$

at $XE1 < x < XE2$, $0 < y < YE(x)$

2) At the interface between the electrode and the weldment (z = L1),

$$-k_w \frac{\partial}{\partial z} T_{w(x,y,L_1)} + \frac{1}{\sigma_e} (\phi_{(x,y,L_1)} - \phi_e)^2 = - k_e \frac{\partial}{\partial z} T_{e(x,y,L_1)} \quad (9b)$$

at $XE1 < x < XE2$, $0 < y < YE(x)$

$$T_{w(x,y,L_1)} = T_{e(x,y,L_1)} \quad (9c)$$

3) On the water-cooled surface of electrode (z = L2),

$$-k_e \frac{\partial}{\partial z} T_{e(x,y,L_2)} = h_w [T_{e(x,y,L_2)} - T_\infty] \quad (9d)$$

4) At all surfaces otherwise specified,

$$\frac{\partial T}{\partial n} = 0 \quad (9e)$$

Numerical Solution Method

To examine the shunt effect, an analysis of the current density distribution based upon the voltage and temperature distributions has to come first. Furthermore, to overcome the difficulties in the analysis, the subsequent finite difference method is employed.

Grid for Numerical Calculation

When the shunt effect is taken into consideration, the two-dimensional axisymmetric formulation by Cho (Ref. 9) cannot be applied since the voltage distribution and the temperature distribution are not symmetric due to the shunt effect. Hence, here three-dimensional rectangular coordinates and the corresponding finite difference grid are employed.

The finite difference grid geometry used for the numerical calculation is shown in Fig. 4. The mesh concentration is done near the nugget-forming part since high current density results in a large variation in both voltage and temperature distributions. To avoid tremendous computational burdens, the existing preweld nugget (shunt circuit, dotted line in Fig. 3) is simplified as an equivalent rectangular (solid line) of the same cross-sectional area. (See assumption 5 in the section on voltage potential distribution.)

Finite Difference Equation

The governing Equations 5, 7 and 8 and the corresponding boundary conditions are discretized into appropriate finite difference equations. The finite difference equation for Equation 5, which represents the voltage distribution in the weldment, is obtained by applying the principle of the conservation of current flow to the arbitrary node in the weldment. We denote the following:

$$I_{(i-1)jk} + I_{(i+1)jk} + I_{i(j-1)k} + I_{i(j+1)k} + I_{ij(k-1)} + I_{ij(k+1)} = 0 \quad (10)$$

where

$$I_{(i-1)jk} = \frac{2}{\sigma_{(i-1)jk} + \sigma_{ijk}} \Delta y_{(j)} \, \Delta z_{(k)} \frac{\phi_{(i-1)jk} - \phi_{ijk}}{\Delta x_{(i-1)}} \quad (11a)$$

$$I_{(i+1)jk} = \frac{2}{\sigma_{(i+1)jk} + \sigma_{ijk}} \Delta y_{(j)} \, \Delta z_{(k)} \frac{\phi_{(i+1)jk} - \phi_{ijk}}{\Delta x_{(i)}} \quad (11b)$$

$$I_{i(j-1)k} = \frac{2}{\sigma_{i(j-1)k} + \sigma_{ijk}} \Delta x_{(i)} \, \Delta z_{(k)} \frac{\phi_{i(j-1)k} - \phi_{ijk}}{\Delta y_{(j-1)}} \quad (11c)$$

$$I_{i(j+1)k} = \frac{2}{\sigma_{i(j+1)k} + \sigma_{ijk}} \Delta x_{(i)} \, \Delta z_{(k)} \frac{\phi_{i(j+1)k} - \phi_{ijk}}{\Delta y_{(j)}} \quad (11d)$$

$$I_{ij(k-1)} = \frac{2}{\sigma_{ij(k-1)} + \sigma_{ijk}} \Delta x_{(i)} \, \Delta y_{(j)} \frac{\phi_{ij(k-1)} - \phi_{ijk}}{\Delta z_{(k-1)}} \quad (11e)$$

$$I_{ij(k+1)} = \frac{2}{\sigma_{ij(k+1)} + \sigma_{ijk}} \Delta x_{(i)} \, \Delta y_{(j)} \frac{\phi_{ij(k+1)} - \phi_{ijk}}{\Delta z_{(k)}} \quad (11f)$$

where I_{ijk} denotes the current at the node (i,j,k), ϕ_{ijk} is an approximation of the voltage potential, ϕ, σ_{ijk} is a local resistivity dependent on the local temperature of the node (i,j,k) and Δx, Δy and Δz are the step sizes in x, y and z directions, respectively. The ϕ_{ijk} for each node in the above equations is obtained by the Douglas formula, which is a kind of alternating direction implicit (ADI) method, taking advantage of numerical stability (Ref. 14).

In analyzing the unsteady temperature distribution in the weldment and electrode, the finite difference equations corresponding to Equations 7 and 8 are obtained by applying the principle of energy conservation to the arbitrary node:

$$\rho_{ijk}\, c_{ijk} \frac{T_{ijk,n+1} - T_{ijk,n}}{\Delta t} V_{ijk} = Q_{(i-1)jk} + Q_{(i+1)jk} + Q_{i(j-1)k} + Q_{i(j+1)k} + Q_{ij(k-1)} + Q_{ij(k+1)} + \dot{Q}_{ijk} \quad (12)$$

where ρ_{ijk}, c_{ijk} and V_{ijk} denote density, specific heat and volume of the node (i,j,k), respectively. $T_{ijk,n}$ is the temperature of the node at the time $t = n\Delta t$, and Q_{ijk} denotes the heat flux at the node (i,j,k) and is shown below:

$$Q_{(i-1)jk} = \frac{k_{(i-1)jk} + k_{ijk}}{2} \Delta y_{(j)} \Delta z_{(k)} \frac{T_{(i-1)jk,n} - T_{ijk,n}}{\Delta x_{(i-1)}} \quad (13a)$$

$$Q_{(i+1)jk} = \frac{k_{(i+1)jk} + k_{ijk}}{2} \Delta y_{(j)} \Delta z_{(k)} \frac{T_{(i+1)jk,n} - T_{ijk,n}}{\Delta x_{(i)}} \quad (13b)$$

$$Q_{i(j-1)k} = \frac{k_{i(j-1)k} + k_{ijk}}{2} \Delta x_{(i)} \Delta z_{(k)} \frac{T_{i(j-1)k,n} - T_{ijk,n}}{\Delta y_{(j-1)}} \quad (13c)$$

$$Q_{i(j+1)k} = \frac{k_{i(j+1)k} + k_{ijk}}{2} \Delta x_{(i)} \Delta z_{(k)} \frac{T_{i(j+1)k,n} - T_{ijk,n}}{\Delta y_{(j)}} \quad (13d)$$

$$Q_{ij(k-1)} = \frac{k_{ij(k-1)} + k_{ijk}}{2} \Delta x_{(i)} \Delta y_{(j)} \frac{T_{ij(k-1),n} - T_{ijk,n}}{\Delta z_{(k-1)}} \quad (13e)$$

$$Q_{ij(k+1)} = \frac{k_{ij(k+1)} + k_{ijk}}{2} \Delta x_{(i)} \Delta y_{(j)} \frac{T_{ij(k+1),n} - T_{ijk,n}}{\Delta z_{(k)}} \quad (13f)$$

where k_{ijk} denotes the thermal conductivity of the node corresponding to the temperature, $T_{ijk,n}$.

Heat generation $\dot{Q}_{ijk}$ is classified according to the boundary as follows: At the nodes in the weldment and the electrode;

$$\dot{Q}_{ijk} = \frac{1}{\sigma_{ijk}} \left[\left(\frac{\phi_{(i-1)jk} - \phi_{(i+1)jk}}{\Delta x_{(i-1)} + \Delta x_{(i)}} \right)^2 + \left(\frac{\phi_{i(j-1)k} - \phi_{i(j+1)k}}{\Delta y_{(j-1)} + \Delta y_{(j)}} \right)^2 + \left(\frac{\phi_{ij(k-1)} - \phi_{ij(k+1)}}{\Delta z_{(k-1)} + \Delta z_{(k)}} \right)^2 \right] V_{ijk} \quad (14)$$

At the interface between two weldments, denoting A(i,j,k) as the corresponding area;

$$\dot{Q}_{ij1} = \frac{2}{\sigma_w} (\phi_{ij1} - \phi_n)^2 A_{(i,j,1)} \quad (15)$$

At the interface between the weldment and the electrode;

$$\dot{Q}_{ij9} = \frac{1}{\sigma_e} (\phi_{ij9} - \phi_e)^2 A_{(i,j,9)} \quad (16)$$

Simulation

Having obtained the complete finite difference equation, the numerical study on the influence of the shunt mechanism can be theoretically investigated. The investigation includes the effect of the spot spacing on the voltage and the temperature distribution in the weldment with the weld cycle.

For the numerical calculation of the shunt effect, the mesh concentration is performed near the nugget-growing zone in the weldment as shown in Figs. 4A and 4B (shunt spacing = 8 mm). The domain concerned in this study is the weldment volume of $5.5 \times 17.2 \times 1.6$ mm^3, ($0.21 \times 0.68 \times 0.06$ in.^{3}) and an electrode with the height of 4.0 mm (0.16 in.). Although the actual electrode is a cylinder with tapered-flat tip diameter of 5 mm (0.2 in.), its tip is simplified as a combined rectangular bar having contact area bounded by YE(X) as shown in Fig. 3 so as to avoid computational burden. The time step size, Δt, was taken as a half cycle period (8.333 ms) of 60 Hz power supply. In calculating the voltage and the temperature distributions, the Douglas formula, which is a kind of alternating direction implicit (ADI) method, was employed. Its merits of numerical stability and computation time are well explained in Ref. 14.

In calculating the voltage distribution in the weldment, the voltage drop between the electrode and the interface of the weldment, ϕ_e, must be measured and substituted into the boundary conditions (Equation 6). The voltage drop was measured as explained in the next section with a weld-checker (MM-502A, Miyachi Electric Co.), the outputs of which are the averaged value of the welding voltage and current for every half cycle during welding. In calculating the voltage distribution, the effect of the electrode force on the contact resistance is also taken into account, using Equation 3. The contact resistivities at room temperature, $\sigma_w(T_o,P)$ and $\sigma_e(T_o,P)$, which are the interfacial resistivities in the weldment and the resistivity in electrode/weldment contact, respectively, were obtained from Ref. 15. The influence of temperature on contact resistivity, thermal conductivity and specific heat, which are contained in Equations 5, 7 and 8, is also taken into consideration, using tables in the ASM *Metals Handbook* (Ref. 2) and polynominal equations derived in Ref. 16. For the phase change problem, the method proposed in Ref. 17 is employed. That is, during fusion, the specific heat, c_w, is assumed to be

$$c_w = \frac{H_\ell}{T_\ell - T_s} \quad (17)$$

since alloy steel has a melting range from the solidus temperature T_s to the liquidus temperature T_ℓ, where H_ℓ is the latent heat of fusion.

Knowledge of the voltage distribution thus obtained enables the total weld current, I, and shunt current, I_s, to be easily computed by the following equations:

$$I = \sum_{e=1}^{N_e} I_e \quad (18)$$

$$I_s = \sum_{a=1}^{N_s} I_a \quad (19)$$

where N_e is the number of mesh at the interface between the weldment and the electrode, N_s is the number of mesh in the adjacent preweld nugget (shunt circuit), and I_e and I_a are the current flows in the mesh corresponding to N_e and N_s, respectively.

In the simulation study, a mild steel plate is used as the weldment and an RWMA Class II electrode with tapered-flat shape is used as a test electrode. The chemical composition and the associated material properties of the weldment and the electrode are well documented in Ref. 9. The simulations were performed for various shunt spacings and welding heat inputs. The simulation results are explained as follows and discussed in detail in comparison to the experimental results.

Experiments

The objective of the experiments is to verify the simulation results of the temperature distribution in the weldment in the presence of the shunt effect. The experiments were performed under the

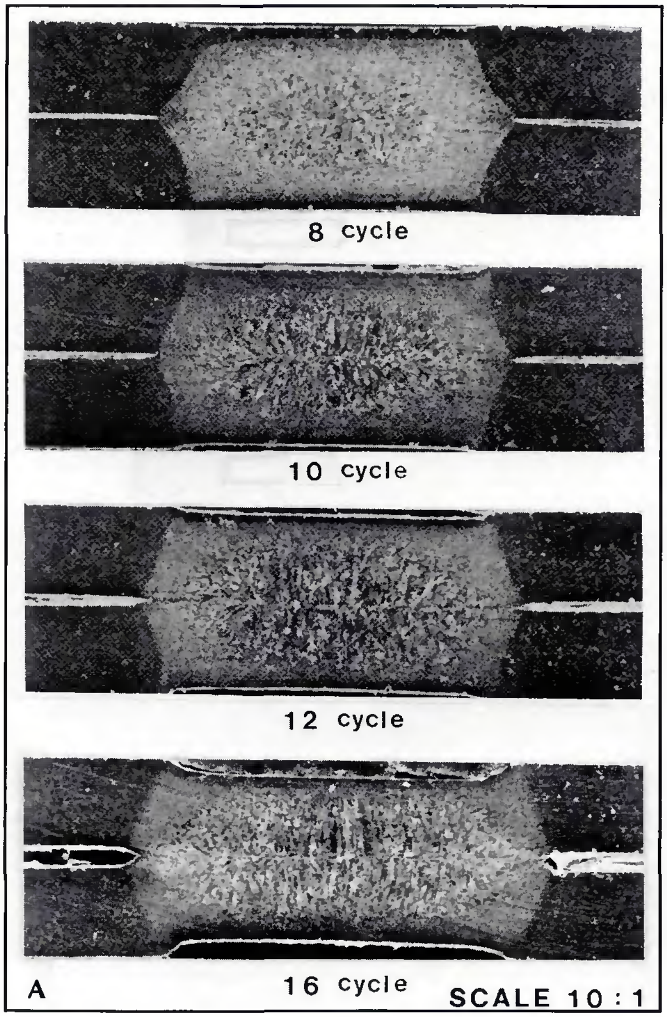

Fig. 5—Photographs of cross-sectioned specimens showing nugget geometry variation with weld time. A—System parameters: electrode force, 360 kgf; weld current, 5.92 kA; shunt spacing, infinity (no shunt effect); B—system parameters: electrode force, 360 kgf; weld current, 5.98 kA; shunt spacing, 8 mm.

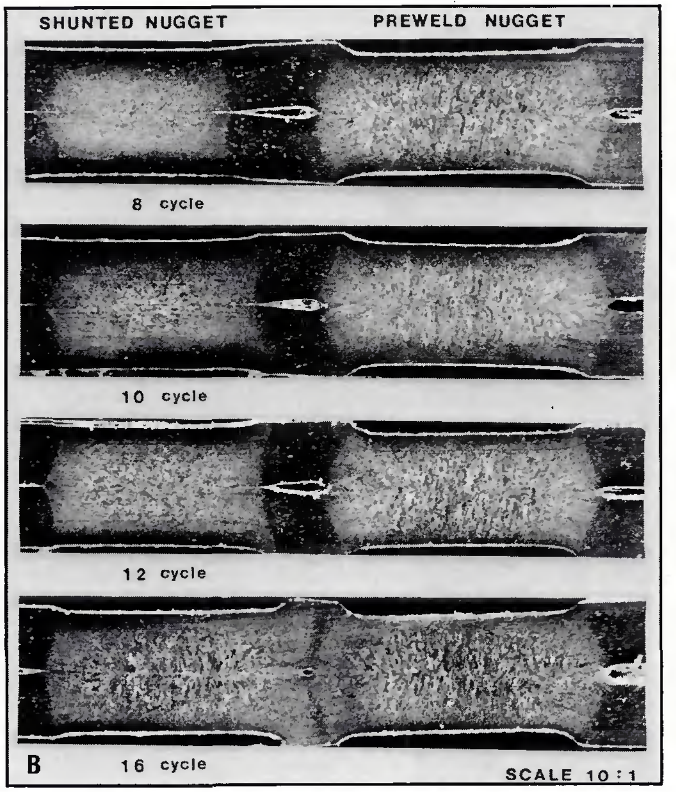

welding conditions corresponding to those used in the simulation study.

Experimental Apparatus

The experiments were carried out on an air-operated resistance spot welding machine (Model SP-AF50, Cho-Heung Welding Company) of rated capacity 50 kVA. The heat input was controlled by adjusting the SCR's firing angle. The squeeze time and the hold time were set as recommended by the Resistance Welding Manufacturers' Association (RWMA). The electrode used was an RWMA Class II with tapered-flat shape and tip diameter of 5 mm. During the welding process, the variations of voltage, current and resistance were monitored using a weld checker (Model MM-502A, Miyachi Electronic Company). This device displays simultaneously the averaged values of the above three variables for every half cycle.

Experimental Procedures

The experiment was conducted to investigate a variation of the temperature distribution in the weldment with the shunt effect. To examine the effect of the shunt spacing on the temperature distribution, the welding time was fixed at 16 cycles, the electrode force at 360 kgf, and the weld current at 4.7 kA and 5.9 kA while the shunt spacings were varied as 8 mm (0.31 in.), 20 mm (0.78 in.), and infinity (no shunt effect). The weldments used in these experiments were the same as those used in the simulation. These specimens were degreased with toluene to maintain a uniform surface condition.

For every cycle of welding, the welding voltage and current were measured using the weld checker. In order to obtain temperature distribution in the weldment, some specimens were prepared with these subsequent treatments after welding: 1) sectioning along the center of the nugget, 2) mounting and polishing, and 3) etching with 5% Nital solution. From inspection of the micro- and macrophotographs of the sectioned specimens, two distinct isothermal lines of solidus temperature (1493°C/2719°F: boundary of the dendrite structure) and A_1 transformation point (723°C/1328°F: boundary of the HAZ) in the weldment were observed by a metal microscope of 1 μm resolution.

Experimental Results

Figure 5A shows a typical macrostructure in the cross-sectioned specimens after the microetching procedure. It can be observed in the macrophotographs that the weldment has three different structures. The first, which occupies the middle part of the weldment, is a dendrite structure that appears in the nugget when the molten metal is solidified. The next region encircling the nugget is the heat-affected zone (HAZ) where the austenite is partially transformed into martensite that is developed with rapid cooling from above the A_1 transformation point. The metallurgical structure outside the HAZ remains unaffected by heat. From the above metallurgical considerations, we can obtain at least two isothermal lines of solidus temperature (1493°C: boundary of the dendrite structure) and A_1 transformation points (723°C: boundary of the HAZ) on the microphotograph of the prepared specimens (Figs. 5A and 5B). In Fig. 5B, an unsymmetric metallurgical structure due to shunt current and resulting heat generation can be seen. In addition, these results are explained fairly well and compared

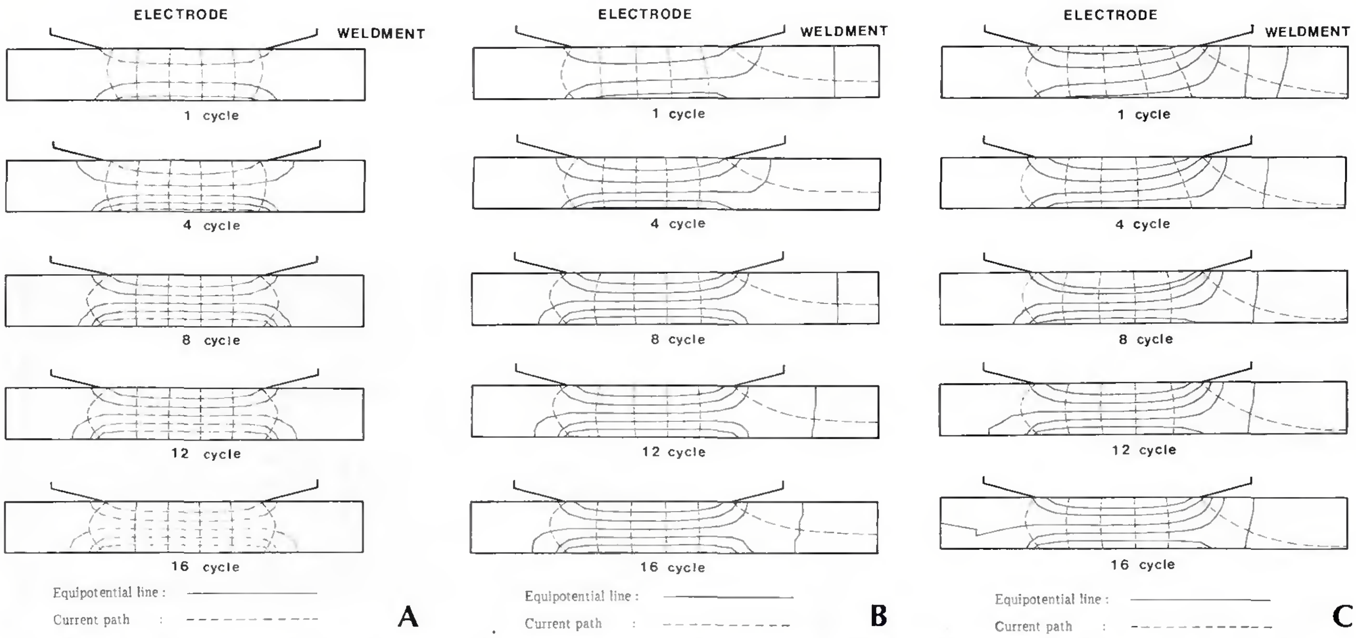

Fig. 6 — Voltage distribution and schematic current path with weld time. A — Electrode force, 360 kgf; weld current, 5.92 kA; shunt spacing, infinity (no shunt effect); B — electrode force, 360 kgf; weld current, 5.98 kA; shunt spacing, 20 mm; C — electrode force, 360 kgf; weld current, 5.98 kA; shunt spacing, 8 mm.

with the numerical prediction in the following section.

Comparison between Theory and Experiment

Voltage Distribution vs. Shunt Spacing

The variation of the voltage distribution in the weldment vs. the spot spacing is illustrated in Figs. 6A through 6C. These simulation results show fairly clearly the effect of the shunt mechanism. In Fig. 6A, with no adjacent nugget, the equipotential lines and the schematic current paths in the weldment show axisymmetric distribution. However, in Figs. 6B and 6C, with the shunt effect being taken into account, an unsymmetrical voltage distribution and current path due to the shunt circuit made by the adjacent weld can be seen. With the adjacent weld, the voltage distribution near the edge of the electrode contact shows a rather steep gradient to the direction of the shunt circuit — Fig. 6C (cycles 1, 4 and 8). This results in relatively higher current density, producing more heat and as illustrated in Fig. 7C, while at the interface between the weldments a similar voltage gradient develops to the opposite direction of the shunt current. As shown in Figs. 6C and 7C, this also results in high current density and heat generation in the early stage of the weld cycle (until cycle 8). Another observation in Figs. 6B and 6C is that the voltage distribution in the weldment tends to have the equipotential lines parallel to the interface between the weldments as the weld cycle goes by after cycle 8. This is mainly due to a gradual decrease in the contact resistance between the two weldments (nugget-forming zone) and the resulting relatively higher current into the contact area compared to the current into the shunt area. The observed unsymmetrical voltage distribution and the current path are notable with an 8-mm shunt spacing — Fig.

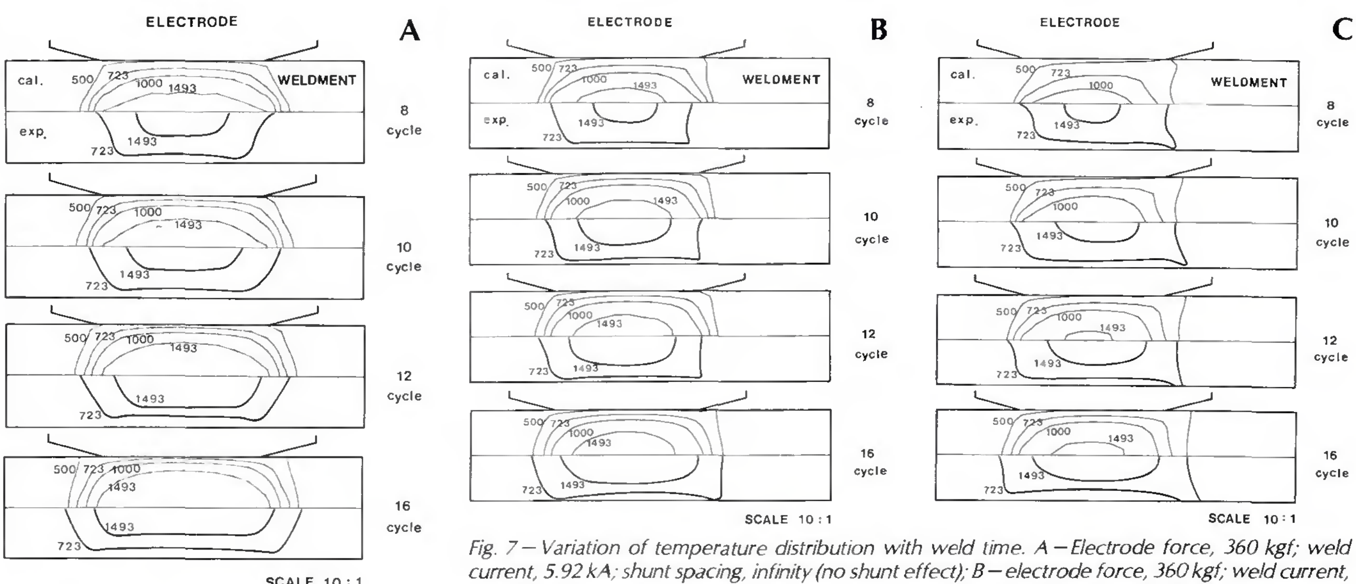

Fig. 7 — Variation of temperature distribution with weld time. A — Electrode force, 360 kgf; weld current, 5.92 kA; shunt spacing, infinity (no shunt effect); B — electrode force, 360 kgf; weld current, 5.98 kA; shunt spacing, 20 mm; C — electrode force, 360 kgf; weld current, 5.98 kA; shunt spacing, 8 mm.

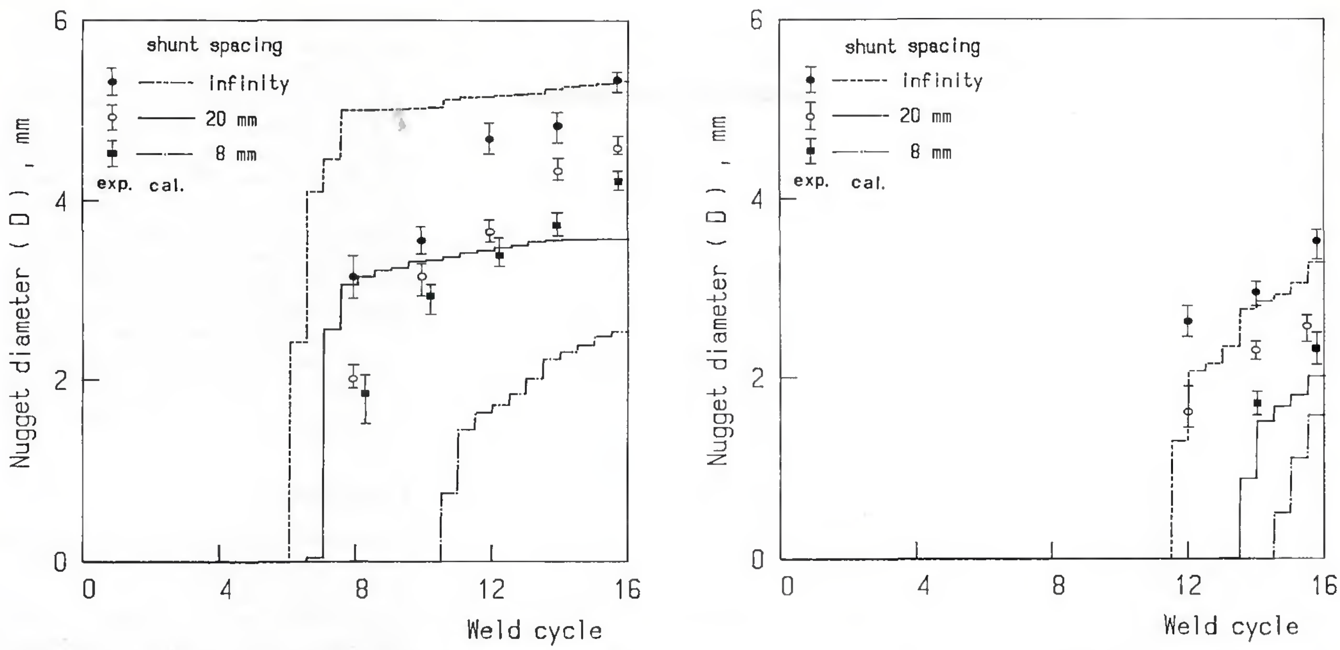

Fig. 8 — Variation of nugget growth behavior with weld time in the presence of shunt effect. A — Electrode force 360 kgf; weldment thickness, 1.6 mm; weld current, 5.9 kA; B — electrode force 360 kgf; weldment thickness, 1.6 mm; weld current 4.7 kA.

6C. But when the spacing is increased to 20 mm (Fig. 6B), this trend is not so dominant in comparison to the case of close spacing. In addition, further increase in the spacing (40 mm/1.6 in.; not shown here) shows nearly symmetrical distribution.

Although experimental verification of the predicted voltage distribution and associated current path could not be attempted, the temperature distribution in the weldment will be influenced by these current paths and voltage distributions as will be explained in detail in the following section.

Temperature Distribution vs. Shunt Spacing

The variation of temperature distribution in the weldment vs. the shunt spacing is illustrated in Figs. 7A through 7C. The figure on the upper half represents the temperature distribution obtained from the numerical calculation and the isothermal lines on the lower half represent the experimental results obtained by the micro-etching test. The experimental results were reconstructed from the photographs of cross-sectioned specimens as illustrated in Figs. 5A and 5B.

In the case of no shunt effect, which is equivalent to the shunt spacing being infinity, Fig. 7A shows the isothermal lines of 723°C (the boundary of the HAZ) and 1493°C (the boundary of the nugget). There is clearly a discrepancy between model prediction and experimental result. The nugget diameter predicted by numerical calculation is larger than that of the experiment. Figs. 7B and 7C show the temperature distributions for the shunt spacings of 20 and 8 mm, respectively. These figures illustrate that the shunt spacing produces an unsymmetrical temperature distribution due to the shunt effect, and the unsymmetric distribution reduces to a symmetric one as the shunt spacing varied from 8 mm to infinity. These results show a similar trend as that obtained for the voltage distribution in the previous section. In Fig. 7C, the isothermal lines are clearly seen to be shifted toward the adjacent preweld nugget (shunt circuit). This is attributable to the fact that due to the shunt current, the resultant heat generation is much higher in the peripheral interface between the electrode and the weldment to the direction of the shunt circuit as discussed in the previous section. Moreover, it can be observed that the predicted temperature distributions are qualitatively consistent with the experimental results.

The differences between the model predictions and the experimental results are probably due to Assumption 3, made in the section on the formulation of the numerical model, which proposes that the boundary of workpiece/workpiece contact area is enlarged along the isothermal line of 723°C as welding progresses. The assumption was to take into account the mechanical collapse in the neighborhood of the melting zone due to softening of the weldment and the electrode load. In an actual RSW process, the two weldments are distorted outward by electrode squeeze force and thus the contact area can hardly be predicted without considering mechanical deformation. The discrepancies are also attributable to the fact that this model only allows the current flow through the previous adjacent spot and the incipient spot under the electrodes. In actual welding, conduction of the welding current is not so localized initially, but rather occurs over a large area. Only when some deformation occurs, effectively reducing the interfacial resistance to a smaller value, does the current flow become restricted.

Nugget Growth Behavior vs. Shunt Spacing

Based on the numerical calculation of the temperature distribution in the previous section, nugget growth behavior with the shunt effect during welding can be examined. The isothermal line of 1493°C was considered as the nugget boundary. Thus, the nugget diameter can be calculated, and its growing behavior with the weld cycle can be analyzed.

As the temperature rises, local melting begins at the center of the workpiece/workpiece interface and a molten nugget develops outwards. At the same time, heat is being lost, primarily by conduction into the electrodes. As the nugget boundary gets closer to the electrode/workpiece interface, its growth slows down due to heat loss into the interface. Therefore, based on this reasoning, the nugget growth mechanism can be described in three distinct stages: 1) Some incubation period before which no melting is observed. 2) A region of rapid growth. 3) A region over which the rate of nugget growth is progressively decreased.

The nugget growth behavior predicted by the proposed numerical model can be well interpreted in terms of these three stages, provided that sufficient heat is supplied, which is the case of d_s = infinity and d_s = 20 mm in Fig. 8A. In case of dominant shunt effect, insufficient heating

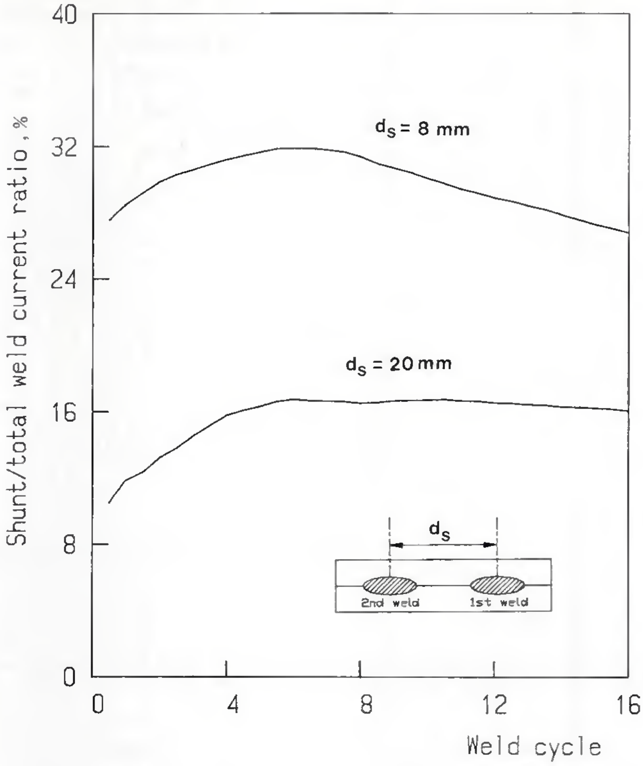

Fig. 9 — Variation in the ratio of shunt current to total weld current for two cases of shunt spacing: electrode force, 360 kgf; weldment thickness, 1.6 mm; weld current, 5.9 kA.

cannot be avoided due to leakage in the welding current, and the third stage was not observed as shown in Fig. 8A (d_s = 8 mm) and in Fig. 8B.

To verify the numerical prediction of the nugget growth behavior, the weld specimens were obtained by actual welding under the conditions corresponding to those of numerical calculation. The nugget diameter was measured by a sectioning, mounting, polishing and micro-etching procedure, as explained previously. The mean (black dot), maximum and minimum diameters were obtained as shown in Figs. 8A and 8B. Each mean value in two figures is averaged data from the ten measured nugget diameters.

As indicated in many previous works (Refs. 3-6, 18, 19) on the shunt effect, a smaller nugget diameter is obtained due to leakage in weld current to the shunt circuit. The numerical calculations and the measured results are in good agreement in the sense that the closer the shunt spacing, the smaller the nugget diameter obtained. This trend is true of two different welding current conditions as shown in Figs. 8A and 8B. However, differences in the calculated nugget diameters and the measured values are clearly shown in the two figures. As discussed in the previous section, the main cause of the discrepancies is thought to be Assumption 3 made in the formulation of the numerical model concerning the initial contact area and the enlargement of contact area between two weldments. The differences in the nugget diameters are also attributable to an insufficient number of mesh of the three-dimensional FDM model due to common block memory overflow in programming with the CYBER computer.

Shunt Current vs. Shunt Spacing

Figure 9 shows the variation in the ratio of the shunt current to total weld current with the weld cycle for two cases of the shunt spacing. A notable fact in this calculated result is that a maximum of 32% of the total weld current is shunted through the adjacent weld in the case of shunt spacing, d_s = 8 mm. This is the main cause of the shunt mechanism, which deteriorates weld quality as a result of a reduction in effective weld current. Another finding is that the shunt current increases until cycle 7 and decreases thereafter. This phenomenon is probably due to the fact that, until cycle 7, a greater increase in bulk resistance of the weldment in the region of direct path, which results from continuing heat generation, causes an increase in the shunted current. After cycle 7, both the almost-steady temperature distribution in the weldment in the direction of the z-axis and the reduction in the contact resistance at the weldment/weldment interface (faying surface) cause an increase in effective welding current through the incipient spot, thus a gradual decrease in the shunt current can be explained as the weld cycle goes by.

The shunt spacing of 20 mm produces a similar trend in the case of the 8-mm spacing, but there is a difference in the amount of the shunt current. This is due to an increase in the resistance of the shunt circuit as the shunt spacing is varied from 8 to 20 mm. It can be easily understood that the infinite shunt spacing has no shunt effect, and this is identical to the case of a single spot weld. Although experimental verification of this prediction could not be attempted due to the difficulty in measuring exactly the shunt current in the case of close shunt spacing (8 and 20 mm), these results will provide some physical insights into understanding the shunt mechanism and can be used as an analytical tool for the design of a weld schedule that compensates for an undersized nugget in the RSW process.

Conclusions

The effect of the shunt mechanism on the weld quality has been investigated using an analytical thermal-electric model. This model can predict its effect upon the variation of voltage potential and temperature distribution in the weldment. It takes into account the dependence of material properties such as thermal conductivity, specific heat and resistivity in the weld material on the temperature variation. The effect of the thermal-electric interaction at the welding interface is also included in the proposed model. Based upon this model, the voltage and the temperature distributions, which vary with the shunt spacing, are numerically obtained via a finite difference method. To verify the validity of the proposed model and the simulation results, a series of experiments was conducted under the same welding conditions as used in the simulation. Both results are relatively in good agreement, although there are some differences between the measured nugget size and the calculated one. The compensation of the shunt effect by regulating the weld current based upon this numerical model will be possible. To improve this model, further work is needed to describe the variation of the contact area on the faying surface, which is a major unsolved problem in the RSW process.

References

1. *Metals Handbook*. 1971. Welding and brazing, 8th ed., Vol. 6, ASM International, Materials Park, Ohio.

2. *Metals Handbook*. 1978. Physical properties of carbon- and low-alloy steel, 9th edition, Vol. 1, ASM International, Materials Park, Ohio.

3. Hard, A. R. 1948. Preliminary test of spot weld shunting in 24ST Alcald, *Welding Journal* 27(6):491-495.

4. Blair, R. H. 1947. Shunt circuit impedance in spot welding 1/8-, 1/4- and 1/2-in. mild steel. *Welding Journal* 26(10):843-848.

5. Nippes, E. F., Savage, W. F., and Robelotto, S. M. 1955. Measurement of shunting currents in series spot welding 0.036-in. steel.

Welding Journal 34(6):618-s to 624-s.
6. Johnson, I. W., 1960. Spot welding of carbon steel, *Welding Journal* 39(1):89-s to 96-s.
7. Nied, H. A., 1984. The finite element modeling of the resistance spot welding process. *Welding Journal* 63(4):123-s to 132-s.
8. Gould, J. E. 1987. An examination of nugget development during spot welding, using both experimental and analytical techniques. *Welding Journal* 66(1):1-s to 10-s.
9. Cho, H. S., and Cho, Y. J. 1989. A study on the thermal behavior in resistance spot welds. *Welding Journal* 68(6)236-s to 244-s.
10. Holm, R. 1967. *Electric Contacts*. Springer-Verlag, N.Y.
11. Tslaf, A. L. 1982. A thermophysical criterion for the weldability of electric contact material in a steady-state regime. *IEEE Tran. CHMT*, Vol. CHMT-5, No. 1, March, pp. 147–152.
12. O'Neil, H. 1967. *Hardness Measurement of Metals and Alloys*. 2nd Edition, Champman and Hall, London, England, pp. 153–188.
13. Cunningham, A. J. R., Begeman, M. L., and Short, B. E. 1966. An analysis of the nugget formation in projection welding. *Welding Journal* 45(7):305-s to 313-s.
14. Carnahan, B., Luther, H. A., and Wilkes, J. O. 1969. *Applied Numerical Methods*. John Wiley and Sons, N.Y.
15. Kim, J. W. 1984. A study on thermal behavior and voltage potential field formation of weldment in resistance welding. M.S. thesis, Department of Production Engineering, KAIST, Seoul, Korea.
16. Yamamoto, T., and Okuda, T. 1971. A study of spot welding of heavy-gauge mild steel. *Welding in the World* Vol. 9, No. 7/8, pp. 234–255.
17. Bonacia, C., Comini, G., Fasano, A., and Primicerio, M. 1973. Numerical solution of phase-change problems. *Int. J. Heat Mass Transfer*, 16, pp. 1825–1832.
18. Yeon, J. S. 1986. A study on the shunt effect in resistance spot welding process. M.S. thesis, Department of Production Engineering, KAIST, Seoul, Korea.
19. Chang, H. S. 1989. In-process monitoring and control of weld nugget geometry for resistance spot welding process. Ph.D. thesis, Department of Production Engineering, KAIST, Seoul, Korea.

Appendix A

C_e	specific heat of electrode
C_w	specific heat of weldment
L_1	thickness of weldment
L_2	distance from the center of weldments to water-cooled surface
h_w	convection heat transfer coefficient to water
H	hardness of material
H_ℓ	latent heat of fusion
i	node number in x direction
j	node number in y direction
k	node number in z direction
J	current density vector
k_e	thermal conductivity of electrode
k_w	thermal conductivity of weldment
q	heat generation at the interface
Δt	time increment in numerical analysis
T_e	temperature of electrode
T_w	temperature of weldment
T_ℓ	liquidus temperature of weldment
T_s	solidus temperature of weldment
T_∞	temperature of cooling water
T_o	room temperature
Δx	grid size in x direction
Δy	grid size in y direction
Δz	grid size in z direction
ρ_e	density of electrode material
ρ_w	density of weldment material
σ	resistivity of weldment
σ_c	interfacial resistivity of material
σ_e	interfacial resistivity in electrode/weldment contact
σ_w	interfacial resistivity in weldment/weldment contact
ϕ	voltage potential
ϕ_e	voltage potential at the electrode
ϕ_n	voltage potential at the center of the interface between two weldments
ϕ_{ijk}	approximation of ϕ at node (i,j,k) in numerical analysis
$T_{ijk,n}$	approximation of local temperature, T, at node (i,j,k) at time t = n Δt
I_{ijk}	approximation of current, I, at node (i,j,k)
Q_{ijk}	heat flux at node (i,j,k)
$\dot{Q}_{ijk}$	heat generation at node (i,j,k)

Appendix B

Numerical Values of the Isopotential Contours in Figs. 6A, B and C

Table 1 (Shunt spacing = infinity, Fig. 6A)

Weld cycle	Highest value equivalent to top isopotential line [Volt]					
1	[0.198]	0.165	0.132	0.099	{0.066}	{0.033}
4	[0.333]	0.278	0.222	0.167	0.111	0.056
8	[0.385]	0.321	0.257	0.193	0.128	0.064
12	[0.384]	0.320	0.256	0.192	0.128	0.064
16	[0.370]	0.308	0.247	0.185	0.123	0.062

Table 2 (Shunt spacing = 20 mm, Fig. 6B)

Weld cycle	Highest value equivalent to top isopoetntial line [Volt]					
1	[0.183]	0.153	0.135	0.092	0.061	(0.031)
4	[0.312]	0.260	0.208	0.156	0.104	(0.052)
8	[0.381]	0.318	0.254	0.191	0.127*	0.064
12	[0.307]	0.256	0.205	0.154	0.102*	0.051
16	[0.272]	0.227	0.181	0.136	0.091*	0.045

Table 3 (Shunt spacing = 8 mm, Fig. 6C)

Weld cycle	Highest value equivalent to top isopotential line [Volt]					
1	0.162	0.135	0.108	0.081	0.054	0.027
4	[0.258]	0.215	0.172	0.129	0.086	0.043
8	[0.306]	0.255	0.204	0.153	0.102	0.051*
12	[0.301]	0.251	0.201	0.151	0.100	0.050*
16	[0.288]	0.240	0.192	0.144	0.096	0.048*

* — drawn by two isopotential lines.
( ) — not drawn since the corresponding isopotential lines are outside of the right boundary of the weldment.
[ ] — not drawn since the corresponding isopotential lines almost coincide with the upper contacting boundary of the weldment.
{ } — not drawn since the corresponding isothermal lines almost coincide with the lower contacting boundary of the weldment.

WRC Bulletin 343
May 1989

Destructive Examination of PVRC Weld Specimens 202, 203 and 251J

This Bulletin contains three reports:

(1) Destructive Examination of PVRC Specimen 202 Weld Flaws by JPVRC
By Y. Saiga

(2) Destructive Examination of PVRC Nozzle Weld Specimen 203 Weld Flaws by JPVRC
By Y. Saiga

(3) Destructive Examination of PVRC Specimen 251J Weld Flaws
By S. Yukawa

The sectioning and examination of Specimens 202 and 203 were sponsored by the Nondestructive Examination Committee of the Japan Pressure Vessel Research Council. The destructive examination of Specimen 251J was performed at the General Electric Company in Schenectady, N.Y., under the sponsorship of the Subcommittee on Nondestructive Examination of Pressure Components of the Pressure Vessel Research Committee of the Welding Research Council. The price of WRC Bulletin 343 is $24.00 per copy, plus $5.00 for U.S., or $8.00 for overseas, postage and handling. Orders should be sent with payment to the Welding Research Council, Room 1301, 345 E. 47th St., New York, NY 10017.

WRC Bulletin 352
April 1990

In October 1987, the PVRC Steering and Technical Committees on Piping Systems established a task group on independent support motion (ISM) to evaluate the technical merits of using the ISM method of spectral analysis in the design and analysis of nuclear power plant piping systems.

The results of the task group evaluation culminated in a unanimous technical position that the ISM method of spectral seismic analysis provides more accurate and generally less conservative response predictions than the commonly accepted envelope response spectra (ERS) method, and are reported in this WRC Bulletin. The price of WRC Bulletin 352 is $25.00 per copy, plus $5.00 for U.S., or $10.00 for overseas, postage and handling. Orders should be sent with payment to the Welding Research Council, 345 E. 47th St., Room 1301, New York, NY 10017.

WRC Bulletin 353
May 1990

Position Paper on Nuclear Plant Pipe Supports

This position paper recommends design methods which represent the collective "best methods" of the industry. These enhanced design methods are developed by reviewing the issues that have added to the complexity of design and fabrication of piping systems.

Publication of this report was sponsored by the Task Group on Nuclear Plant Pipe Supports of the Technical Committee on Piping Systems of the Pressure Vessel Research Council of the Welding Research Council. The price of WRC Bulletin 353 is $25.00 per copy, plus $5.00 for U.S., or $10.00 for overseas, postage and handling. Orders should be sent with payment to the Welding Research Council, 345 E. 47th St., Room 1301, New York, NY 10017.